THE JOURNAL OF PHYSICAL CHEMISTRY C
A JOURNAL OF THE AMERICAN CHEMICAL SOCIETY

pubs.acs.org/JPCC
Article

Mechanism of Benzene Hydroxylation on Tri-Iron Oxo-Centered Cluster-Based Metal−Organic Frameworks

Jenny G. Vitillo,* Madhuresh Choudhary, Matthew C. Simons, Laura Gagliardi, and Aditya Bhan*

Cite This: J. Phys. Chem. C 2023, 127, 23246−23257
Read Online

ACCESS | Metrics & More | Article Recommendations | Supporting Information

ABSTRACT: High-valent Fe(IV)-oxo species derived upon reactions of N_2O with Fe(II) centers—embedded in the framework of tri-iron oxo-centered-based metal−organic frameworks (MOFs)— selectively affect the conversion of benzene-to-phenol via electrophilic addition to arene C−H bonds akin to oxygen transfer mechanisms in the P450 enzyme. The Fe(II) species identified by Mössbauer spectroscopy can be titrated in situ by the addition of NO to completely suppress benzene oxidation, verifying the relevance of Fe(II) centers. Observed inverse kinetic isotope effects in benzene hydroxylation preclude the involvement of H atom transfer steps from benzene to the Fe(IV)-oxo species and instead suggest that the electrophilic iron-oxo group adds to an sp^2 carbon of benzene, resulting in a change in the hybridization from sp^2-to-sp^3. These mechanistic postulates are affirmed in Kohn−Sham density functional calculations, which predict lower barriers for additive mechanisms for arene oxidation than H atom abstraction steps. The calculations show that the reaction proceeds on the pentadectet spin surface and that a non-innocent ligand participates in the transfer of the H atom. Following precedent literature which demonstrates that these Fe(IV)-oxo species react with C−H bonds in alkanes via hydrogen atom abstraction to form alcohols, it appears that iron(IV)-oxo species in MOFs exhibit duality in their reactions with inert hydrocarbon substrates akin to enzymes—if the C−H bonds are in saturated aliphatic hydrocarbons, then activation occurs via hydrogen abstraction, while if the C−H bonds are aromatic, then activation occurs by addition rearrangement.

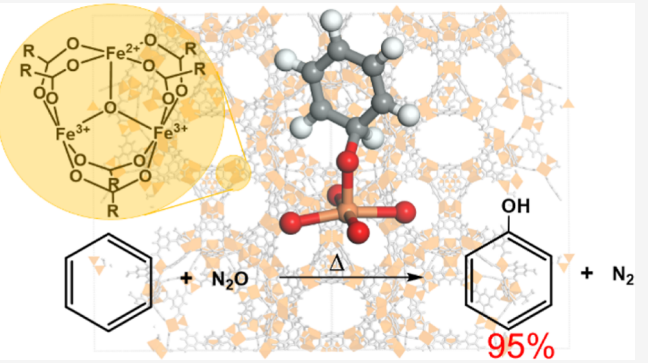

1. INTRODUCTION

Metal−organic frameworks (MOFs) with reactive centers embedded in the framework provide an organized array of noninteracting, well-defined catalytic centers that are uniform in composition and placement.[1] Following precedent literature in zeolites,[2,3] Fe embedded in the MOFs, based on tri-iron oxo-centered metal nodes (e.g., MIL-100 and PCN-250, see inset in Figure 1a) has been shown to form open five-coordinated Fe(II) sites that react stoichiometrically with N_2O to form Fe(IV)═O species similar to those reported for enzymes.[4−6] These species can readily activate strong, apolar C−H bonds in short aliphatic hydrocarbons (CH_4, C_2H_6, and C_3H_8) with the formation of the corresponding alcohols.[7−14] Tri-iron oxo-centered cluster-based MOFs are also characterized by exceptional chemical and thermal stability.[15] Additionally, simple and highly scalable synthetic protocols have been reported for these MOFs.[16] Previously, we have reported[7,8] that the so-formed high-spin open Fe(II) centers in Materials Institute Lavoisier (MIL)-100(Fe) and PCN-250(Fe) react with N_2O to form high-valent Fe(IV)═O species, which are short-lived and highly reactive. Their high reactivity makes direct observation of Fe(IV)═O elusive, as shown by the in situ spectroscopic study performed by Xiao et al.[14] on similar species in $Fe_{0.1}Mg_{1.9}(dobdc)_2$. This Fe(IV)═O is an entatic state in which the weak ligand field induced by the carboxylate linkers and structural constraints induced by the MOF lattice result in a metal-oxo species that is facile at H atom abstraction from apolar C−H bonds in alkanes. The Fe(II) species formed upon thermal treatment of the MOF, which serve as the precursor to the Fe(IV)═O species, can be readily identified by Mössbauer, X-ray absorption, and NO probe molecule infrared adsorption spectroscopy, and the number of such sites can be enumerated by chemical titration under reaction conditions.[7,8] The cleavage of aliphatic C−H bonds by Fe(IV)═O species proceeds in single-turnover events via hydrogen abstraction followed by radical rebound mechanisms[7−12,14] as in heme and nonheme enzymes,[4−6,17] resulting in the oxidation of CH_4-to-CH_3OH and of C_3H_8 to C_3H_6 and to C_3H_7OH. Partial oxidation products are formed with selectivity exceeding 60−75% at conversions exceeding

Received: September 26, 2023
Revised: November 8, 2023
Accepted: November 9, 2023
Published: November 24, 2023

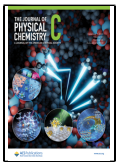

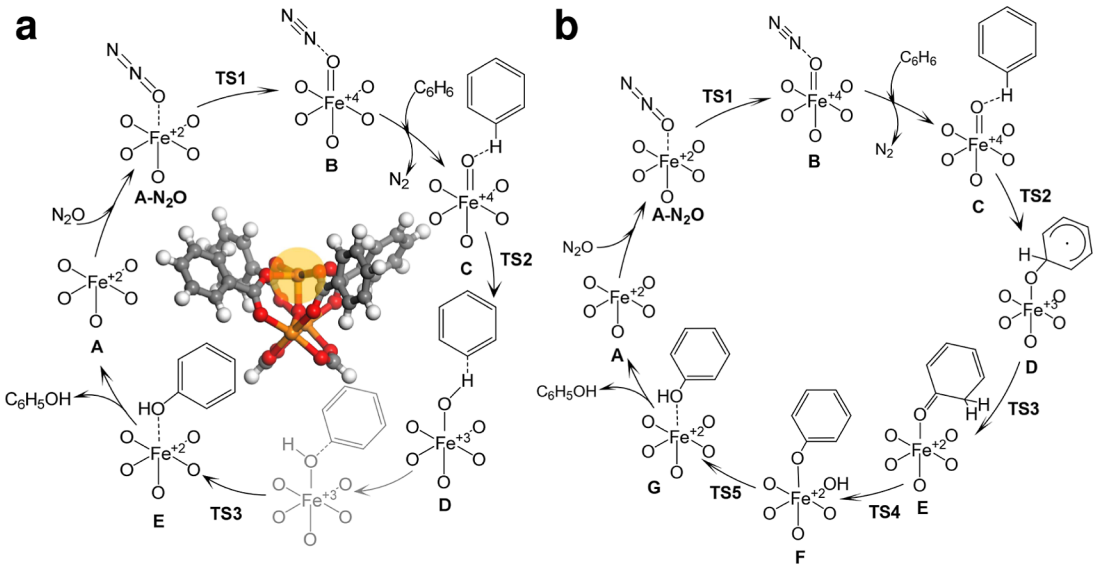

Figure 1. Schematics for the conversion of benzene to phenol on divalent Fe(II) sites in MIL-100(Fe) following (a) a hydrogen abstraction pathway followed by radical rebound (**habs**) or (b) an oxygen addition-rearrangement pathway without passing through the formation of benzene oxide (**addrear1**). Parts of the cycles considered in the present work are reported in black. In part (a), the structure of the **A** cluster is also reported, as optimized at the UM06-L/def2-TZVP level ($2S + 1 = 15$). Color code: red (oxygen), gray (carbon), orange (iron), and white (hydrogen). Reacting iron is highlighted with a yellow circle.

25% in stoichiometric reaction events, with the desired products of selective oxidation recovered upon washing the MOF postreaction.

Aromatic hydroxylation is another important class of reactions catalyzed by Fe(IV)=O sites in enzymes as a means of detoxification and excretion of toxic arenes.[18−21] If a selective direct oxidation process for the conversion of benzene to phenol can be developed, it will eliminate the cosynthesis of acetone in the state-of-the-art industrial cumene process.[22] Iron-based enzymes catalyze benzene hydroxylation using molecular oxygen as the oxidant in catalytic sequences initiated by electrophilic addition of high-valent iron-oxo species to π-bonds in benzene (step **C** to **D** in Figure 1b),[4,5,21,23,24] without direct interaction with C−H bonds. Decay of the resulting σ-complex occurs in a manner that retains the original hydrogen of the activated C−H bond via migration of the substituent from the site of hydroxylation to the adjacent carbon, the so-called "NIH shift" (NIH from the US National Institute of Health that first reported on it, step **D** to **E** in Figure 1b).[25,26] A similar mechanism has been proposed to occur on the extra-framework Fe centers in zeolites.[27] However, to our knowledge, such a mechanism has not been demonstrated for abiotic heterogeneous catalysts containing Fe in the framework; in particular, no Fe-based MOFs have been reported to affect the direct oxidation of benzene to phenol using N_2O as the oxidant.

Here, we demonstrate using a combination of Mössbauer spectroscopy, chemical titration, isotopic substitution, and Kohn−Sham density functional theory (DFT) calculations that Fe(II) species embedded in the framework of MIL-100 convert benzene to phenol with high selectivity (>95%) via electrophilic addition, akin to what is observed for enzymatic systems. MOFs thus provide an ideal platform for investigating electronic and structural factors in heterogeneous catalysts relevant to selective oxidation of recalcitrant C−H bonds.

2. METHODS

2.1. Experimental Methods. *2.1.1. N_2 Isotherms.* The surface area of MIL-100(Fe) (STREM, USA) samples before and after the reaction was obtained by measuring N_2 isotherms at 77 K using an ASAP 2020 surface area and porosity analyzer (Micrometrics). Samples were degassed at 423 K for 4 h prior to sample analysis, with surface areas determined by using the Langmuir model[28,29] in the standard pressure range ($0.05 < p/p_0 < 0.20$). All the reported quantities were affected by an error of 10%.

2.1.2. Powder XRD. X-ray diffraction (XRD) patterns were collected in the 5−50° 2θ range in the Bragg−Brentano geometry using a laboratory diffractometer (Rigaku SmartLab SE) (step size of 0.01°, time per step 10 s). A Cu Kα anode (Kα, λ = 1.5406 Å) operated at 45 kV and 40 mA was used as the radiation source. The simulated patterns were obtained from previously reported cif files (Crystallography Open Database entry 7102029) and processed using Mercury software (Mercury 2022.1.0, CCDC).

2.1.3. Mössbauer Spectroscopy. ^{57}Fe Mössbauer spectra were recorded at low temperatures (18 K) with samples cooled with liquid helium. Approximately 25 mg of the MIL-100(Fe) sample was mixed with 25 mg of boron nitride (Sigma-Aldrich). One sample was tested after reaction in benzene/N_2O mixtures (2 and 90 kPa) at 523 K, with the sample sealed with Swagelok quick-connect fittings and transferred to a N_2-filled glovebox to prevent air exposure. In the glovebox, the sample was mixed with boron nitride and loaded into a sample holder sealed with parafilm before being transferred to the spectrometer.

2.1.4. Reaction Experiments. The reaction experiments were carried out in a recirculating batch reactor system with a reactor volume of 67 cm^3. In a typical experiment, 53 mg of MIL-100(Fe) powder (STREM, USA) was loaded into a vertical 1/4 in. OD quartz reactor tube. The MOF was supported by plugs of quartz wool above and below the reactor bed and held in place by a 1/16 in. K-type thermocouple

https://doi.org/10.1021/acs.jpcc.3c06423
J. Phys. Chem. C 2023, 127, 23246−23257

(Omega Engineering) from above and a 1/8 in. quartz rod at the bottom. The temperature in the reactor was controlled using the thermocouple, which provided a signal to the PID temperature controller (Watlow, EZ Zone), which in turn adjusted the power to an electric furnace (National Electric Furnace, FA 120, 120 V). A concentric copper block surrounding the reactor was used to minimize axial temperature gradients over the length. A schematic of the batch reactor set up with external recycle is shown in the Supporting Information (Section S8).

The MIL-100(Fe) sample was activated under vacuum (<3 Pa) at 523 K for 10 h, with the sample being heated from ambient temperature to 523 K at a rate of 0.033 K s^{-1}, and subsequently the sample cooled to the reaction temperature (398 K). Mass flow controllers (instruments) were calibrated using a volumetric soap-film flow meter and used to control the flow of helium (Matheson, UHP Enable 99.999%), argon (Matheson, Research Purity 99.9999%), and nitrous oxide (Matheson, USP grade 99%). Benzene (Sigma-Aldrich, HPLC grade, 99.9%) was fed through a syringe pump (KD Scientific).

For the in situ NO titration experiments pursued to identify and count the number of accessible active sites, nitric oxide (Matheson, CP grade 99%) was injected into the reactor system through a dosing chamber (volume 0.1 cm^3) through a 6-way valve (VICI Valco) prior to exposing MIL-100(Fe) to the reaction gas mixture of nitrous oxide and benzene.

The composition of the reactor effluent was quantified by gas chromatography (Agilent, 6890N) using a thermal conductivity detector and a flame ionization detector fitted with HP plot Q (Agilent) and CP Molsieve 5 A (Agilent) columns in series. The reactant gas mixture was recirculated at a rate of 1.17 cm^3 s^{-1} with a recirculation pump (Metal Bellows, MB-21). Online GC sampling was done to determine effluent gas compositions.

To terminate the reaction, the reactor was purged by flowing helium through the reactor bed at a rate of 0.83 cm^3 s^{-1} for 30 min, and then the MOF was removed and washed with D_2O (Cambridge Isotopes Limited) containing acetonitrile as an internal standard. The liquid containing MIL-100(Fe) was transferred to a centrifuge tube fitted with a 0.2 μm filter. The MOF sample was separated from the solution by using a microcentrifuge (operated at 6000 rpm). Desorbed products in solution were quantified using ^{1}H NMR (Ascend 400, Bruker, 400 MHz, 64 scans, td 2 s).

2.1.5. KIE Measurements. A mixture of $^{13}C_6H_6$ (Cambridge Isotope Limited) and $^{12}C_6D_6$ (Sigma-Aldrich) in a ratio of 1.47:1 was used to carry out the reaction. Benzene pressures in the range of 3−5 kPa were selected to maximize rates while still maintaining operation in the vapor phase (benzene vapor pressures ∼10 kPa at ambient temperature). The postreaction MOF sample was washed with H_2O, and the products eluted in solution were analyzed with mass spectroscopy (Agilent technologies GC 7890B fitted with a 7200 QTOF-MS and DB-5 column) to determine the isotopologue distribution.

2.2. Computational Methods. *2.2.1. Density Functional Calculations.* All calculations were performed using the Gaussian 16 program.[30] The M06-L[31] density functional in its unrestricted formalism (U) was used in combination with the def2-TZVP basis sets.[32,33] This level of theory has been shown to accurately describe the electronic structure of single iron centers in ethane and methane oxidation studies[34] and of the tri-iron oxo-centered cluster[9] when compared to multireference wave function theory. Unfortunately, it overestimates by 30% the enthalpy of benzene oxidation with N_2O to phenol and N_2 with respect to the experimental value (−184 vs −261 kJ mol^{-1}),[35] in analogy with B3-LYP/def2-TZVP (−175 kJ mol^{-1}), used in a similar study.[36] The hybrid Minnesota functional M06 (27% Hartree−Fock exchange), although providing a better agreement, still overestimates the reaction enthalpy by 50 kJ mol^{-1}. Nevertheless, the use of M06-L/def2-TZVP was dictated by its reliability in predicting the activation barrier of N_2O activation for MIL-100(Fe) when benchmarked against experiments.[8] For what concerns the present benzene-to-phenol reaction, this level of calculations predicts the kinetic isotope effect (KIE) in very good agreement with the experiments (see below), further validating the use of this level of calculations for modeling tri-iron oxo-centered-based MOFs. The cluster used to model the tri-iron metal node was carved from the periodic structure of the tri-iron oxo-centered MOF, MIL-127, optimized using the Perdew−Burke−Ernzerhof functional[37] as implemented in the VASP 5.4.4 program,[38] with long-range dispersion interactions considered using the scheme proposed by Grimme (D3).[39] The cluster consists of the inorganic subunit of the MOF, terminated by four benzoate groups and two formate groups ($Fe(III)_2Fe(II)(\mu_3\text{-}O)(C_6H_5COO)_4(COO)_2$, see Figure 1a). The four benzoate groups were placed around the reactive iron center to model eventual $\pi-\pi$ interactions occurring between the substrate and the MOF. The positions of the C atoms of the phenyls were kept fixed to model the constraint associated with the presence of the MOF.

Geometry optimizations were carried out by means of the Berny optimization algorithm with an analytical gradient. A (99,590) pruned grid was used (i.e., 99 radial points and 590 angular points per radial point). Gaussian 16 default convergence thresholds were set for optimization. All the energetic data have been corrected for the basis set superposition error (BSSE) following the a posteriori method proposed by Boys and Bernardi,[40] as implemented in Gaussian 16. The BSSE corrected values are indicated by a c superscript and were obtained from the computed Y values as $Y^c = Y +$ BSSE.

Unscaled, harmonic vibrational frequencies were computed analytically. Enthalpies and Gibbs free energies were calculated at 1 atm and 298 K from a conventional ideal gas, rigid rotor, particle in a box, and quantum mechanical harmonic oscillator partition functions, except that the low vibrational frequencies (<50 cm^{-1}) were replaced by a cutoff value (50 cm^{-1}) following the De Moor scheme[41] to account for limitations in the harmonic oscillator approximation for very low-frequency vibrations.[42−46]

Kinetic isotope effect studies for the replacement of all hydrogen atoms in benzene by deuterium atoms were evaluated using the approach discussed by De Visser and coworkers[47−49] using the semiclassical Eyring model

$$KIE_E = e^{(\Delta G^{TS}_{C_6D_6} - \Delta G^{TS}_{C_6H_6})/RT} \quad (1)$$

where ΔG^{TS} is the free energy of activation, R is the gas constant, and T is the temperature (298 K). They also report a KIE value further corrected using the tunneling corrections reported by Wigner (KIE_W)[47−49] by multiplying KIE_E for the tunneling ratio

https://doi.org/10.1021/acs.jpcc.3c06423
J. Phys. Chem. C 2023, 127, 23246−23257

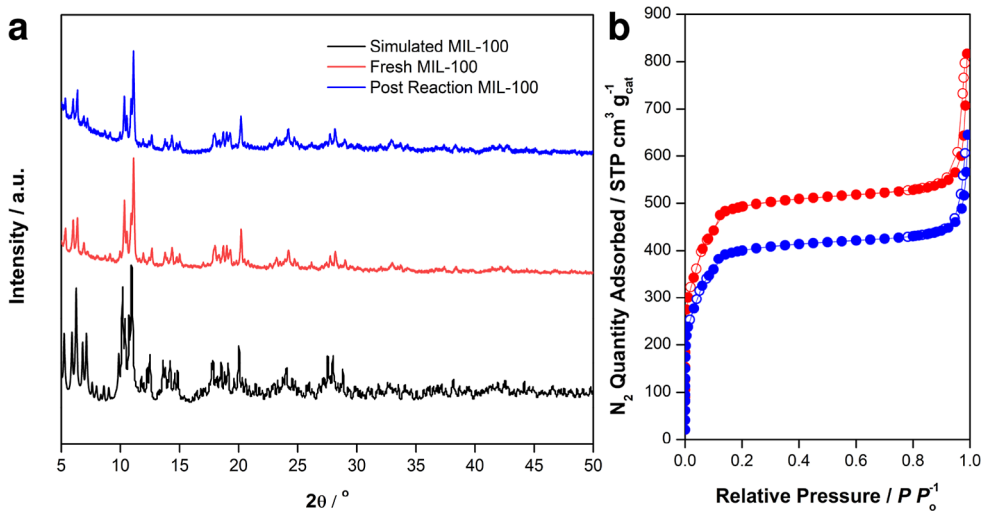

Figure 2. (a) PXRD patterns of MIL-100 as-received (red), after reaction (blue), and reference patterns (black) for MIL-100(Fe). Reaction conditions: the sample was activated at 523 K in vacuo for 10 h before exposure to 90 kPa N_2O + 2 kPa C_6H_6 at 398 K for 2 h, followed by washing with D_2O ex situ. (b) N_2 isotherms of MIL-100(Fe) taken before (red curve, surface area (Langmuir) = 2106 $m^2\ g^{-1}$) and after (blue curve, surface area (Langmuir) = 1729 $m^2\ g^{-1}$) reaction. Samples were degassed at 513 K, and isotherms were collected at 77 K.

$$\frac{Q_{t,H}}{Q_{t,D}} = \frac{1+\frac{\left(\frac{h\nu_{imm,C6H6}}{kT}\right)^2}{24}}{1+\frac{\left(\frac{h\nu_{imm,C6D6}}{kT}\right)^2}{24}} = \frac{24+\left(\frac{h\nu_{imm,C6H6}}{kT}\right)^2}{24+\left(\frac{h\nu_{imm,C6D6}}{kT}\right)^2} \quad (2)$$

In this equation, h is Planck's constant, k is Boltzmann's constant, and ν_{imm} is the imaginary frequency in the **TS2** transition state.

3. RESULTS AND DISCUSSION

Following our prior work for alkane activation on high-valent Fe-oxo species formed upon exposing tri-iron oxo-centered metal nodes in MIL-100(Fe) and PCN-250(Fe) to N_2O,[7,8] here we investigate the reactions of framework Fe(II) species in mixtures of N_2O and benzene to determine reaction sequences for activation of recalcitrant arene C−H bonds with Fe(IV)═O species. The C−H bonds in benzene are even stronger than those in methane (472.5 kJ mol^{-1} versus 435 kJ mol^{-1} in CH_4)[50] and are not susceptible to direct electrophilic attack. However, unlike σ C−H bonds in methane, the C−H bonds in benzene are susceptible to oxidative addition because of the participation of aromatic π-orbitals in bonding to the metal-oxo species. Experimental and computational studies for benzene hydroxylation by the enzyme cytochrome P450[3,4,19−22] note that high-valent iron oxyl species react with benzene via electrophilic addition to form a σ-complex based on an initial attack on the π-system of the benzene. This σ-complex decays to phenol via inter- or intramolecular mechanisms, retaining the hydrogen in the C−H that was activated, the so-called "NIH shift". Here, we combine spectroscopic and kinetic experimental studies with DFT calculations to illustrate that Fe(IV)═O species in MOFs, similar to P450 enzymes,[5,21] readily react with aromatic C−H bonds via oxidative addition pathways and selectively form phenol.

3.1. Material Characteristics and Reaction Scheme.

The MIL-100(Fe) sample was confirmed to be crystalline by its XRD pattern, which also the as-received material is the MIL-100 phase (see Figure 2a).[16,51] The porosity of the material was determined by nitrogen adsorption at 77 K and is in line with previous reports (see Figure 2b).[7,8,16] The structural integrity of the sample after the reaction was assessed by XRD and N_2 adsorption studies, showing that the material retained high porosity (see Figure 2a,b). Further, the N_2 isotherms do not evidence the formation of mesopores. The decrease in the surface area observed after the reaction (∼10%), although within the uncertainty of the measurement, can also be associated with impurities of the diluent used in the reactor (silica), which could not be completely eliminated from the postreaction sample. These characteristics mimic those we have reported in independent studies for MIL-100(Fe) samples that we used for examining reactions of N_2O with CH_4 and C_3H_8.[7,8]

The chemical characteristics of the Fe species in the MOF were probed by Mössbauer spectroscopy. MIL-100(Fe) samples undergo autoreduction upon thermal treatment when subjected to high temperatures (>473 K) in vacuo, notably resulting in the formation of high-spin Fe(II) sites.[7,8,15,52−55] Accordingly, the Mössbauer spectrum of MIL-100(Fe) after thermal activation at 513 K in vacuum in Figure 3 clearly exhibits an additional doublet characteristic of high-spin (S = 2) Fe(II) species with an isomer shift of ∼1 mm s^{-1} and quadrupole splitting of ∼1.9 mm s^{-1}. The presence of high-spin Fe(II) and Fe(III) species is in line with previous reports on MIL-100(Fe) and amorphous Fe-BTC.[15,52−54]

Exposure of thermally activated MIL-100(Fe) to mixtures of N_2O and benzene at 398 K in a recirculating gas phase batch reactor resulted in the production of N_2 and trace amounts of CO_2 in the gas phase (Figure 4). Individual reaction runs were quenched at durations of 1, 2, and 3 h. The MOF was washed with D_2O ex situ, and the species present in the extract were quantified by ^1H NMR. These data show that benzene-to-phenol oxidation occurs with ≥95% selectivity on a carbon basis and that N_2O consumed to form N_2 and Fe(IV)═O is quantitatively utilized to affect benzene-to-phenol conversion as opposed to oxidation of benzene to CO_2. The present MOF shows a selectivity (>95%) mimicking that of enzymes and higher than that of iron-containing zeolites for prolonged times of reaction (<30%).[56] An additional advantage is the absence

https://doi.org/10.1021/acs.jpcc.3c06423
J. Phys. Chem. C 2023, 127, 23246−23257

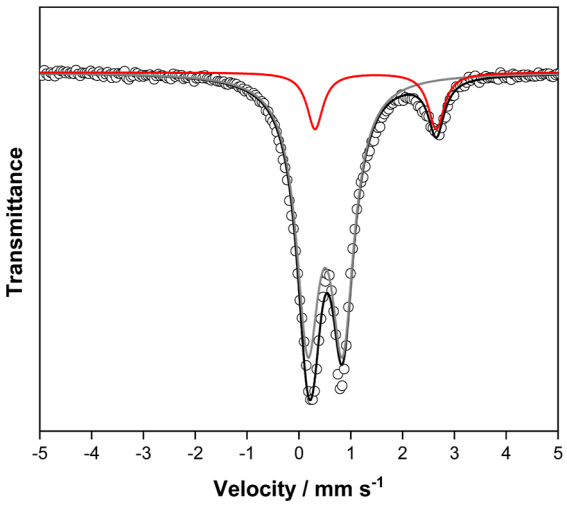

Figure 3. Mössbauer spectra of MIL-100 material treated to 513 K in vacuum and transferred to a spectrometer without exposure to the atmosphere. Spectra were collected at 18−20 K. Open circles—raw data, black line—fit to raw data curves for identified Fe species. Gray line—Lorentzian doublet assigned to an Fe(III) species (δ = 0.52 mm s^{-1}, ΔE_Q = 0.67 mm s^{-1}). Red line—Lorentzian doublet assigned to an Fe(II) species (δ = 1.5 mm s^{-1}, ΔE_Q = 2.3 mm s^{-1}).

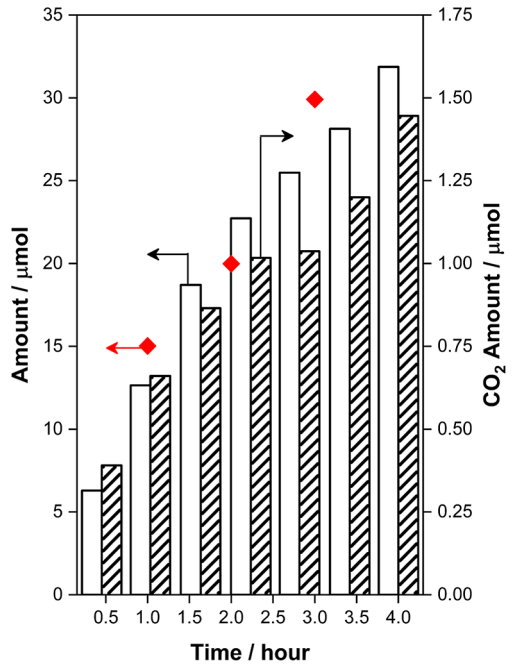

Figure 4. Yield of gas phase products in a batch reactor for a N_2O + C_6H_6 experiment with 53 mg of MIL-100(Fe), 398 K, $P_{total,t=0}$ = 110 kPa, $P_{N_2O,t=0}$ = 90 kPa, and $P_{C_6H_6,t=0}$ = 2 kPa. All products were estimated by GC analysis, while phenol was estimated by NMR analysis after washing the MOF with D_2O (striped bars: CO_2, white filled bars: N_2, and red diamonds: phenol).

of coke formation that affects the reaction catalyzed by iron-containing zeolites.[57]

The relevance of Fe(II) species was probed in chemical titration studies similar to those we have reported previously for CH_4 and C_3H_8 oxidation.[7,8] Briefly, NO binds more strongly to Fe(II) than to Fe(III) species[2,55,58] (108 vs 56 kJ mol^{-1} in MIL-100):[55] if Fe(II) species are relevant for reaction, then the addition of NO should inhibit the rate.

For chemical titration of benzene oxidation reactions, we performed a series of experiments in which a known amount of NO was preadsorbed on the MIL-100(Fe) after it was activated in vacuo at 473 K and, subsequently, measured the amount of phenol with ^{1}H NMR after quenching the reaction and washing the sample with D_2O. The results for this series of five independent titration experiments with varying amounts of preadsorbed NO are shown in Figure 5, noting that ∼340

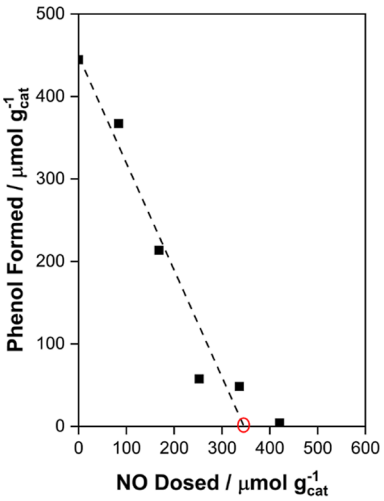

Figure 5. Moles of phenol formed (black squares) in the batch reactor as a function of NO dosed to the MOF before exposure to the reaction mixture (90 kPa of N_2O and 2 kPa of benzene) at 398 K for 2 h. The estimated number of Fe(II) centers accessible under the reaction conditions is 340 μmol g_{cat}^{-1} consistent with the estimate from Mössbauer analysis (about 325 μmol g_{cat}^{-1}, open red circle).

μmol g_{cat}^{-1} of Fe(II) is relevant for reaction, considering that each adsorbed NO can titrate one Fe(II) center. The amount of Fe(II) assessed from Mössbauer studies (∼325 μmol g_{cat}^{-1}) is also shown on this plot, to note the quantitative agreement between the Fe(II) concentration assessed from in situ chemical titration and ex situ Mössbauer studies.

Collectively, the structural and chemical characterization and the kinetic data discussed above allow us to infer that iron embedded in the framework of tri-iron oxo-centered MOFs is highly selective for single-turnover benzene hydroxylation reactions and these reactions involve Fe(II) species that react with N_2O to form the oxidant. These experiments, however, do not allow us to infer whether H atom abstraction (**habs** in Figure 1a) or electrophilic addition to form a σ-complex (**addrear1** in Figure 1b and **addrear2** in Figure S1) occurs during the course of the reaction. Besides the signature "NIH shift" associated with arene oxidation by Fe(IV)=O species (**D** to **E** step in Figure 1b), another characteristic distinct for oxidative addition mechanisms for arene oxidation is the small or inverse kinetic isotope effect (KIE ≈ 1). KIE values of ∼0.9 were reported for benzene hydroxylation by nonheme iron-(IV)-oxo complexes $[Fe(IV)(Bn\text{-}tpen)(O)]^{2+}$ and $[Fe(IV)(N4Py)(O)]^{2+}$ by de Visser and co-workers,[47] KIE values of 0.95−1.25 have been observed for the oxidation of deuterated chlorobenzenes,[59] and KIE values of 1.04−1.16 were reported by Solomon and co-workers[27] for benzene-to-phenol conversion on iron-containing zeolites by the Fe(IV)=O species associated with α-O in these materials. These KIE values preclude the occurrence of hydrogen-atom abstraction because KIEs for H atom abstraction mechanisms significantly exceed

https://doi.org/10.1021/acs.jpcc.3c06423
J. Phys. Chem. C 2023, 127, 23246−23257

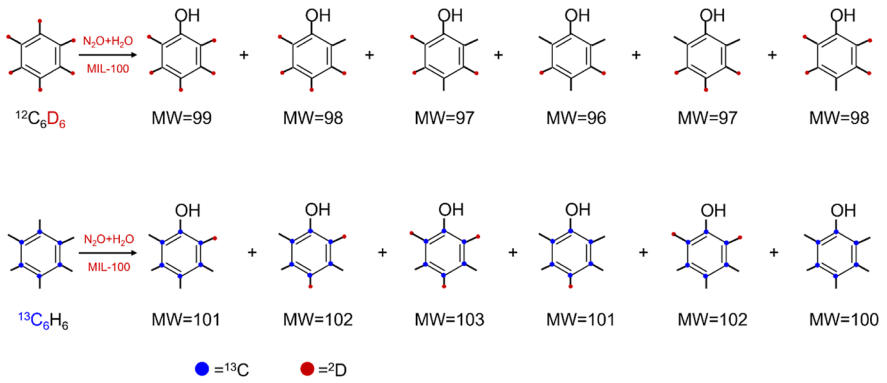

Figure 6. Schematic showing different phenol isotopologues resulting from $^{13}C_6H_6$ and $^{12}C_6D_6$ benzene.

1,[60,61] and, notably, k_H/k_D values of ∼1 suggest a small or inverse kinetic isotope effect in aromatic ring oxidation reactions, which would be consistent with a change in hybridization from sp^2-to-sp^3 occurring during the addition of an electrophilic iron-oxo group to the sp^2 carbon in a benzene ring to form a σ-adduct.[47] We performed a series of experiments to assess the KIE of benzene oxidation on MIL-100(Fe) materials to affirm whether electrophilic addition mechanistically describes benzene hydroxylation on iron-containing MOFs.

Mixtures of $^{13}C_6H_6$ (Cambridge Isotope Limited) and $^{12}C_6D_6$ (Sigma-Aldrich) in a ratio of 1.47:1 were reacted with N_2O over MIL-100(Fe) in three independent experiments, varying the benzene partial pressure (3−5 kPa) while keeping the N_2O pressure at 90 kPa. The products were extracted by washing the MOF with H_2O. The KIE was determined from the isotopologue distribution of phenol as analyzed by mass spectrometry (Agilent technologies GC 7890B fitted with a 7200 QTOF-MS and DB-5 column) based on eqs 3−7. The KIE was assessed assuming first-order kinetics in benzene; the N_2O reaction order does not need to be specified for this calculation

$$r_H = k_H[C_6H_6][N_2O] \quad (3)$$

$$r_D = k_D[C_6D_6][N_2O] \quad (4)$$

$$\mathrm{KIE} = \frac{k_H}{k_D} = \frac{r_H}{r_D}\frac{[C_6D_6]}{[C_6H_6]} \quad (5)$$

where

$$r_H = \sum_{MW=100}^{105} X_{MW} \quad (6)$$

$$r_D = \sum_{MW=94}^{99} X_{MW} \quad (7)$$

MW is the molecular weight (MW is in g mol^{-1} and it is 94 = $^{12}C_6H_5OH$, 99 = $^{12}C_6D_5OH$, 100 = $^{13}C_6H_5OH$, and 105 = $^{13}C_6D_5OH$) and X_{MW} is the mole fraction for isotopologues with $\frac{m}{z}$= MW estimated by MS analysis. The use of $^{13}C_6H_6$ and $^{12}C_6D_6$ precludes any potential overlap in mass of phenol isotopologues by H/D exchange upon washing with H_2O (94 ≤ MW ≤ 99 and 100 ≤ MW ≤ 105, respectively, Figure 6, also see Section S7, Figures S6−S7, and Table S8).

The KIE values evaluated for each of the three independent experiments are reported in Table 1. An inverse KIE (KIE ≈ 0.85) is observed, which excludes the possibility of H atom abstraction and radical rebound mechanisms being relevant for arene hydroxylation. While the reaction order of benzene for benzene hydroxylation was not explicitly measured, an upper bound KIE of ∼1.25 can be determined if the hydroxylation reaction has zero-order kinetics in benzene. As a reference, we note that oxidation reactions that are known to transpire by hydrogen atom abstraction on nonheme Fe(IV)-oxo complexes are characterized by higher KIEs: 1.9 ≤ KIE ≤ 5.9 for the oxidation of methane to methanol in Fe-ZSM-5,[62] while KIE values >30 have been reported for the oxidation of ethylbenzene to benzyl alcohol.[60,61] The inverse KIE we assess is in line with an electrophilic oxidative addition mechanistic sequence that would result in a change from sp^2-to-sp^3 hybridization of the carbon center. In an effort to verify these mechanistic postulates, we pursued a complementary computational study using DFT to compare and contrast the possible modes of C−H activation in arene hydroxylation.

Table 1. KIE Estimated Based on Reactions of $^{13}C_6H_6/N_2O$ and $^{12}C_6D_6/N_2O$ after Exposure to 90 kPa N_2O + 3−5 kPa (Benzene) at 398 K for 2 h, Followed by Washing with H_2O Ex Situ[a]

benzene (C_6H_6) pressure	3 kPa	4 kPa	5 kPa
KIE	0.83	0.84	0.85

[a]The KIE values reported considering the reaction to be first-order with regard to the concentration of benzene.

3.2. Computational Studies. Two competitive pathways were considered in the DFT calculations: (a) hydrogen abstraction followed by radical rebound (**habs**, see Figure 1a) and (b) oxygen addition and rearrangement (**addrear1**, see Figure 1b). Both mechanisms share the formation of a ferryl species through the decomposition of N_2O (**B**), followed by the coordination of benzene (**C**). The **habs** pathway has the following additional steps (see Figure 1a): (i) C−H bond activation with the formation of a benzyl radical (from **C** to **D**), (ii) formation of phenol through radical rebound (from **D** to **E**), and (iii) desorption of phenol, which corresponds to the regeneration of the MOF (from **E** to **A**). The mechanism for the **addrear1** pathway is similar to that reported for zeolites.[27] After **C** formation, **addrear1** proceeds with (i) electrophilic attack of the oxoferryl on benzene with the formation of the σ-complex (**D**); (ii) hydrogen shift from the hydroxylation site to the adjacent carbon, with the formation of a ketone intermediate ("NIH shift", from **D** to **E**); (iii) proton transfer from the dienone to the oxygens of the framework with the formation of phenolate (from **E** to **F**); (iv) reshuttling of the

https://doi.org/10.1021/acs.jpcc.3c06423
J. Phys. Chem. C 2023, 127, 23246−23257

proton to the oxo group and formation of phenol (from **F** to **G**); and (v) desorption of phenol (from **G** to **A**). The corresponding reaction profiles of **habs** and **addrear1** are reported in Figure 7, while the corresponding numerical values are listed in Tables S3−S4.

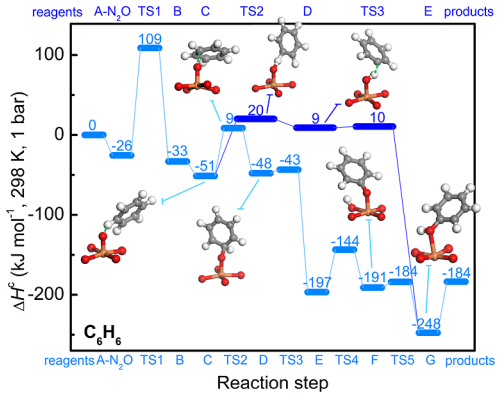

Figure 7. Energy profile reporting phenol formation on the metal node of MIL-100(Fe) through benzene oxidation by N_2O. Reaction mechanisms: **habs** (blue) and **addrear1** (light blue). The **habs** mechanism requires the abstraction of hydrogen from benzene to form a benzyl radical. The **addrear1** pathway is an addition rearrangement mechanism supposing a non-innocent iron ligand that can shuttle a proton to the oxo group. A similar mechanism has also been proposed for other single iron catalysts, i.e., iron zeolites,[27] enzymes,[21] and nonheme iron complexes.[47] Reaction profiles were calculated at the UM06-L/def2-TZVP level on the $2S + 1 = 15$ spin surface. Enthalpies of the separated reactants (the **A** cluster, N_2O, and one benzene molecule) have been set as zero. The optimized structure of the Fe center, its first coordination sphere, and the interacting species are shown for relevant steps. Color code: red (oxygen), gray (carbon), orange (iron), and white (hydrogen).

Alternative to the formation of the σ-complex, oxygen addition can also pass through the formation of an arene oxide.[63,64] Arene oxides are known to isomerize to phenols at physiological pH.[63] Two alternative arene oxide pathways, including the formation of an epoxide as an intermediate, have been suggested in the literature,[20,21,63] here indicated as **daad** and **addrear2** (Figure S4a). There, the benzene oxide is formed from **C** in the **addrear1** mechanism (see Figure 1b) through the insertion of the oxygen on the double bond (direct addition, see **dadd** in Figure S4a) or it is formed from intermediate **D** (**addrear2**, see Figure S4a). The **daad** mechanism has been excluded in both heme[21,63] and nonheme[27,47] single-iron-based catalysts. In tri-iron oxo-centered MOFs, the formation of benzene oxide (**C** → **E′** step) is exothermic by −28 kJ mol^{-1} (see Table S5), i.e., the reaction is favored thermodynamically. Nevertheless, we were not able to locate the transition state **TS2′** of the **daad** pathway, although a very large and diversified set of starting geometries was considered. The transition structure linking **C** with benzene oxide is a second-order saddle point, with two imaginary frequencies: one mode corresponds to oxygen addition and the second mode corresponds to the transition state corresponding to **E′** formation in **addrear2**. Based on these results, we can rule out the **daad** pathway also on MIL-100(Fe), similar to all single-atom iron-based catalysts reported so far.[65] The formation of the epoxide in **daad** (**D′** → **E′** step) is slightly more exothermic than **C** → **E′** in the **addrear2** mechanism (−31 versus −28 kJ mol^{-1}, respectively). The enthalpic barrier associated with transition state **TS3′** is 31 kJ mol^{-1}. This means that benzene oxide can form during the reaction through the **addrear2** mechanism, along the lines of what has been previously reported from computational and experimental studies for heme[21,63] and nonheme[47] catalysts. Nevertheless, the competing **TS3** and **E** in the **D** → **E** reaction in **addrear1** are more stable than **TS3′** and **E′** (by 26 and 117 kJ mol^{-1}, respectively). This means that benzene oxide can form eventually during the reaction through the **addrear2** mechanism, although the competing formation of dienone (**E** in **addrear1**) is decidedly more favored, both from a kinetic and thermodynamic vantage point.

In all the mechanisms considered in the computational study, the rate-determining step is associated with the formation of the ferryl species, as verified also for the cleavage of aliphatic C−H bonds on tri-iron oxo-centered metal nodes in MOFs.[7] The second highest barrier is associated with the **C** → **D** step for both **habs** and **addrear1**, although it corresponds to different reactions in the two pathways: the C−H bond scission in **habs** and the oxygen addition for **addrear1**. The oxygen addition step is akin to that noted for other single Fe-based catalysts.[18,19,27,66] The **C** → **D** step in **habs** is computed to be endothermic by 60 kJ mol^{-1} with an associated enthalpic barrier (ΔH^c_{TS2}) of 71 kJ mol^{-1}. After the formation of the benzyl radical, the reaction proceeded in an almost barrierless fashion with the formation of phenol. For the competing **addrear1** pathway, the **C** → **D** step is computed to be only slightly endothermic (3 kJ mol^{-1}) with a ΔH^c_{TS2} of 60 kJ mol^{-1}. ΔH^c_{TS2} computed for MIL-100 is close to the one reported for a similar mechanism in P450 heme enzyme (73 kJ mol^{-1}),[21] while it is higher than in nonheme Fe(IV)-oxo species in $[Fe(IV)(N4Py)(O)]^{2+}$ (36 kJ mol^{-1})[47] and in Fe-BEA* (barrierless).[27]

In the so-formed σ-complex on MIL-100 (**D** in **addrear1**), the substrate is a radical (see Table S1), and it shares very similar electronic and geometric features with σ-complexes having a radical character formed on other single iron-based catalysts.[8,10,18] The comparison of the α-LUMO orbitals for **C** and **D** (see Figure S2) provides evidence that this step, as expected, corresponds to the donation of an electron from benzene to the molecular orbital, having a main contribution from the $3d_z^2$ orbital of iron. The reaction then proceeds with the formation of 2,4-cyclohexadienone through an NIH shift (**E**). This dienone intermediate is significantly stabilized with respect to **D** by −149 kJ mol^{-1}. Correspondingly, the NIH-shift barrier is very low (5 kJ mol^{-1}, **TS3**). The change of the β-HOMO from **D** to **TS3** and from **TS3** to **E** is reported in Figure S3. The reaction then proceeds via the formation of a phenolate (**E** → **F**) species through a proton-shuttle mechanism mediated by the framework oxygens. This step is slightly endothermic and has an associated barrier of 53 kJ mol^{-1}. The proton is then reshuffled back to the substrate (**F** → **G**) with the formation of phenol. In this case, the process is associated with a barrier of only ∼7 kJ mol^{-1}. The direct involvement of the first coordination shell of iron in the reaction makes it a non-innocent ligand. The cluster oxygens mediate the proton shuttle, enabling the transformation of the surface-bound benzene oxide to phenol. It is noteworthy that Fe species embedded in abiotic heterogeneous frameworks share this detail of the mechanism with completely different classes of catalysts for benzene hydroxylation, having been reported for enzymes,[21] nonheme Fe(IV)-oxo species,[47] and zeolites (Fe-BEA*).[27] This common behavior is surprising

https://doi.org/10.1021/acs.jpcc.3c06423
J. Phys. Chem. C 2023, 127, 23246−23257

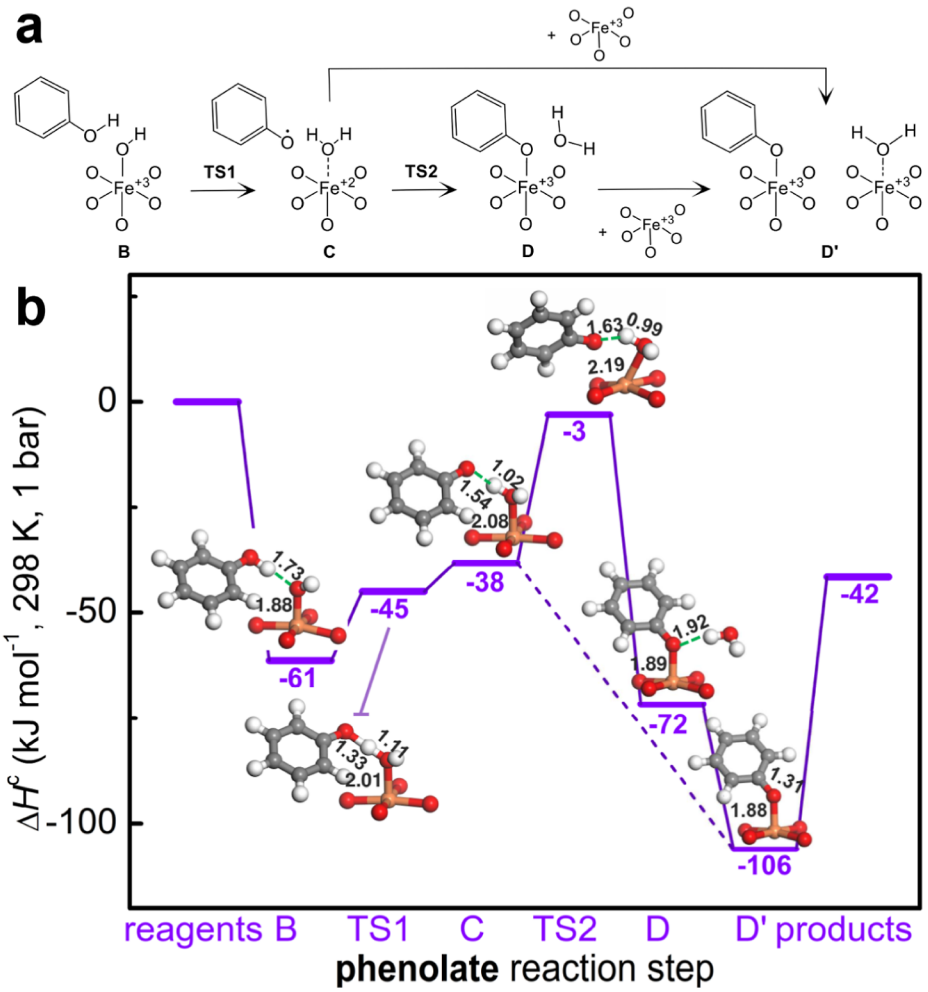

Figure 8. Phenoxy formation from phenol over Fe(III)−OH sites in MIL-100(Fe). (a) Schematics for phenol dehydration via the Fe−O scission pathway. (b) Reaction enthalpy profiles for Fe−O scission dehydration pathways calculated at the UM06-L/def2-TZVP level on the $2S + 1 = 16$ spin surface. Enthalpy of the separated reactants (the hydroxylated form of the **A** cluster and one phenol molecule) was set as zero enthalpy. The optimized structure of the Fe center, its first coordination sphere, and interacting species is shown for each step. Color code: red (oxygen), gray (carbon), orange (iron), and white (hydrogen).

because these compounds, besides the presence of Fe(II) centers, do not share a common chemical composition, dimensionality, or structure and do not have similar accessibility to the metal centers to incoming adsorbates. This finding suggests that Fe(II) centers exhibit common behavior in C−H bond oxidation, independent of the structure that hosts them.

Thus, the results from our calculations noting lower activation and reaction enthalpies for the **addrear1** pathway than the **habs** pathways agree with the experiments pointing toward the electrophilic addition mechanism as kinetically and thermodynamically favored over one involving hydrogen abstraction. Further supporting this assignment, the computed KIE values for the **addrear1** pathway are very close to the experimental values (0.93 and 0.72 for KIE_E and KIE_W, respectively, versus ∼0.85 for the experimental KIE assuming first-order kinetics in benzene). In contrast, the computed KIE_E for the **habs** pathway is 5.12, which is greater than the upper bound KIE of ∼1.25 assuming zero-order kinetics in benzene. The similar KIE values assessed from experiments and computational studies suggest that single iron centers present in the MOFs affect benzene hydroxylation through electrophilic substitution, in analogy with enzymes,[21] homogeneous catalysts,[47] and extraframework iron species in zeolites.[27,62] It is evident from this report and from precedent literature on enzymes and zeolites that Fe(IV)-oxo species exhibit duality in mechanism depending on the nature of the C−H bond to be oxidized, independent of the chemical composition, structure, morphology, or size of the catalyst. Specifically, Fe(IV)-oxo species react with aliphatic C−H bonds via hydrogen atom abstraction to form alcohols, while they activate aromatic C−H bonds by addition-rearrangement. The results of this study allow us to highlight the ability of ferryl species to maintain this characteristic also for a class of Fe-MOFs. This particular characteristic can only be partially attributed to the higher dissociation energy of the Fe(IV)-oxo bond with respect to the other iron ligands because the **addrear** mechanisms require the direct involvement of the ligand. The generality of this observation for MOFs as well as the specific energetic drivers for this duality of C−H bond activation in alkanes and aromatics should be addressed in future studies.

The last step of the reaction is the desorption of phenol to restore the open Fe(II) site (**G** → **A**). This process is endothermic by 64 kJ mol^{-1} (see Figure 7). Phenol binding enthalpy is then large enough to "poison" the Fe(II) centers,

https://doi.org/10.1021/acs.jpcc.3c06423
J. Phys. Chem. C 2023, 127, 23246−23257

being larger than the binding enthalpy of benzene (−33 kJ mol^{-1}) and N_2O (−26 kJ mol^{-1}) to the Fe(II) sites. In analogy with other catalysts,[36,57,67] this could explain the >95% selectivity observed in the experiments, wherein the bound form of phenol avoids its overoxidation.

Protection mechanisms are known to be key in maintaining high selectivity in the methane to methanol reaction and avoiding methanol overoxidation.[6,7,68−70] The formation of stable methoxy species hinders the diffusion of methanol in the gas phase, thus avoiding further oxidation. These methoxy species can be recovered in the form of methanol only by washing the sample postreaction in water. A protection mechanism through the formation of phenolates could explain both the high selectivity and the high thermal stability of the phenol in the MOF. Methoxy species can readily form on acidic surfaces such as zeolites[42−45] and polyoxometalates,[46] through single-step[44,45] or two-step dehydration mechanisms.[42] The activation barriers reported for supports with strong Brønsted acid sites range from 230 kJ mol^{-1} in SAPOs[44] to 80 kJ mol^{-1} in ZSM-22.[42] Simons et al.[7] have recently shown that Fe−OH species formed during the reaction on tri-iron oxo-centered clusters in MOFs allow a similar methanol protection mechanism, although here methoxy species are formed through the deprotonation of methanol because of the low Brønsted acidity of the Fe−OH species. The activation enthalpy of this process in PCN-250 and MIL-100(Fe) is computed to be lower than what is reported for acid surfaces (57 kJ mol^{-1}).[7] We have verified that these Fe−OH species can react with phenol following a mechanism similar to that of methanol, resulting in the formation of Fe-phenolates. The feasibility of this phenol protection mechanism is evident from the DFT reaction profiles reported in Figure 8. The activation barrier for the formation of phenolate by deprotonation of phenol (**B** to **C**) is computed to be only 23 kJ mol^{-1}, i.e., about a third of the activation enthalpy reported for methoxy formation (57 kJ mol^{-1}). The reaction then proceeds downhill with the coordination of phenolate by an open Fe(III) center (**C** to **D′**) or through the displacement of water by the phenolate (**C** to **D**) with an activation barrier of 35 kJ mol^{-1}. Mechanisms for the formation of phenolate from the reaction of phenol with oxygenated iron complexes in Fe-ZSM-5 have also been proposed by Li et al.,[57] with activation energies ranging from 19 to 65 kJ mol^{-1}. This result suggests that deprotonation of hydroxylated species is likely a general protection mechanism in the presence of surface −OH species, independent of the aliphatic or aromatic nature of the substrate. It is important to stress that the formation of Fe-phenolates causes the poisoning of the iron centers while concurrently enhancing the selectivity of the reaction. Phenolates have been suggested to be coke precursors in Fe-ZSM-5.[57] Although a large amount of phenolates are formed in MIL-100(Fe), coke formation was not observed. The absence of coking in MOFs can be associated either with the mononuclearity of Fe sites (not guaranteed in zeolites) or with the lower basicity of the framework oxygen atom in MOFs, which, in turn, limits phenolate formation to the mechanism reported in Figure 8 and excludes coupling/dehydrogenation of more than one phenol molecule per iron site in the MOF.

4. CONCLUSIONS

Fe(II) species embedded in tri-iron oxo-centered clusters of MOFs affect the selective hydroxylation of benzene to phenol in stoichiometric reactions with N_2O. Structural and chemical characteristics of the MIL-100(Fe), probed before and after the reaction using a combination of N_2 uptake, XRD, and Mössbauer spectroscopy, suggest that the material retains its porosity and crystallinity over the course of the reaction and that Fe(II) sites are engendered upon thermal treatment of the MOF. The involvement of Fe(II) sites in benzene hydroxylation is affirmed in chemical titration studies with NO, with rates of benzene hydroxylation being entirely suppressed at NO uptakes of ∼340 μmol g_{cat}^{-1}. Benzene hydroxylation appears to proceed via electrophilic addition, mimicking enzymes, as evidenced by the inverse or small kinetic isotope effect assessed experimentally and verified in Kohn−Sham DFT calculations. Electrophilic addition mechanisms that result in arene hydroxylation on framework Fe-based MOFs are distinct from radical rebound mechanisms that result in aliphatic hydroxylation of aliphatic C−H bonds on these same MOFs. However, the mechanisms that protect the desired product from being overoxidized and that involve dehydrogenation on Fe(III)−OH groups to form persistent surface-bound oxo-species are common for alkane and arene oxidation on Fe-based MOFs. These results suggest that Fe species embedded in microporous materials provide a platform for the design of novel catalysts for the selective hydroxylation of arenes.

■ ASSOCIATED CONTENT

Supporting Information

The Supporting Information is available free of charge at https://pubs.acs.org/doi/10.1021/acs.jpcc.3c06423.

Mass spectrometric analysis data for evaluation of kinetic isotope effects; relevant geometrical, electronic, and energetic parameters for all the structures; and additional energetic plots (PDF)

Cartesian coordinates for the all the optimized geometries (ZIP)

■ AUTHOR INFORMATION

Corresponding Authors

Jenny G. Vitillo − *Department of Science and High Technology and INSTM, Università Degli Studi Dell'Insubria, Como I-22100, Italy;* orcid.org/0000-0002-6213-2039; Email: jg.vitillo@gmail.com

Aditya Bhan − *Department of Chemical Engineering and Materials Science, University of Minnesota, Minneapolis, Minnesota 55455, United States;* orcid.org/0000-0002-6069-7626; Email: abhan@umn.edu

Authors

Madhuresh Choudhary − *Department of Chemical Engineering and Materials Science, University of Minnesota, Minneapolis, Minnesota 55455, United States;* orcid.org/0000-0003-3073-9159

Matthew C. Simons − *Department of Chemical Engineering and Materials Science, University of Minnesota, Minneapolis, Minnesota 55455, United States*

Laura Gagliardi − *Department of Chemistry, Pritzker School of Molecular Engineering, James Franck Institute, University of Chicago, Chicago, Illinois 60637, United States;* orcid.org/0000-0001-5227-1396

Complete contact information is available at: https://pubs.acs.org/10.1021/acs.jpcc.3c06423

Notes

The authors declare no competing financial interest.

■ ACKNOWLEDGMENTS

This work was supported by the Inorganometallic Catalyst Design Center, an Energy Frontier Research Center funded by the U.S. Department of Energy, Office of Science, Basic Energy Sciences, under award no. DE-SC0012702 and by the Catalyst Design for Decarbonization Center, an Energy Frontier Research Center funded by the U.S. Department of Energy, Office of Science, Basic Energy Sciences, under award no. DE-SC0023383. The authors acknowledge the Minnesota Supercomputing Institute (MSI) at the University of Minnesota for providing computational resources. The authors acknowledge Dr. Benjamin Yeh for many helpful technical discussions and for help with tables and figures in this manuscript.

■ ABBREVIATIONS

MIL	Materials Institute Lavoisier
IR	infrared spectroscopy
KS-DFT	Kohn−Sham density functional theory
MOFs	metal−organic frameworks

■ REFERENCES

(1) Rogge, S. M. J.; Bavykina, A.; Hajek, J.; Garcia, H.; Olivos-Suarez, A. I.; Sepulveda-Escribano, A.; Vimont, A.; Clet, G.; Bazin, P.; Kapteijn, F.; et al. Metal-organic and covalent organic frameworks as single-site catalysts. *Chem. Soc. Rev.* **2017**, *46* (11), 3134−3184.

(2) Zecchina, A.; Rivallan, M.; Berlier, G.; Lamberti, C.; Ricchiardi, G. Structure and nuclearity of active sites in Fe-zeolites: comparison with iron sites in enzymes and homogeneous catalysts. *Phys. Chem. Chem. Phys.* **2007**, *9* (27), 3483−3499.

(3) Snyder, B. E. R.; Vanelderen, P.; Bols, M. L.; Hallaert, S. D.; Böttger, L. H.; Ungur, L.; Pierloot, K.; Schoonheydt, R. A.; Sels, B. F.; Solomon, E. I. The active site of low-temperature methane hydroxylation in iron-containing zeolites. *Nature* **2016**, *536*, 317−321.

(4) Shaik, S.; Cohen, S.; Wang, Y.; Chen, H.; Kumar, D.; Thiel, W. P450 Enzymes: Their Structure, Reactivity, and Selectivity—Modeled by QM/MM Calculations. *Chem. Rev.* **2010**, *110* (2), 949−1017.

(5) Shaik, S.; Kumar, D.; de Visser, S. P.; Altun, A.; Thiel, W. Theoretical Perspective on the Structure and Mechanism of Cytochrome P450 Enzymes. *Chem. Rev.* **2005**, *105* (6), 2279−2328.

(6) Vitillo, J. G.; Lu, C. C.; Bhan, A.; Gagliardi, L. Comparing the reaction profiles of single-iron catalytic sites in enzymes and in reticular frameworks for methane-to-methanol oxidation. *Cell Reports Phys. Sci.* **2023**, *4*, 101422.

(7) Simons, M. C.; Prinslow, S. D.; Babucci, M.; Hoffman, A. S.; Hong, J.; Vitillo, J. G.; Bare, S. R.; Gates, B. C.; Lu, C. C.; Gagliardi, L.; et al. Beyond Radical Rebound: Methane Oxidation to Methanol Catalyzed by Iron Species in Metal−Organic Framework Nodes. *J. Am. Chem. Soc.* **2021**, *143* (31), 12165−12174.

(8) Simons, M. C.; Vitillo, J. G.; Babucci, M.; Hoffman, A. S.; Boubnov, A.; Beauvais, M. L.; Chen, Z.; Cramer, C. J.; Chapman, K. W.; Bare, S. R.; et al. Structure, Dynamics, and Reactivity for Light Alkane Oxidation of Fe(II) Sites Situated in the Nodes of a Metal−Organic Framework. *J. Am. Chem. Soc.* **2019**, *141* (45), 18142−18151.

(9) Vitillo, J. G.; Bhan, A.; Cramer, C. J.; Lu, C. C.; Gagliardi, L. Quantum Chemical Characterization of Structural Single Fe(II) Sites in MIL-Type Metal−Organic Frameworks for the Oxidation of Methane to Methanol and Ethane to Ethanol. *ACS Catal.* **2019**, *9* (4), 2870−2879.

(10) Vitillo, J. G.; Lu, C. C.; Cramer, C. J.; Bhan, A.; Gagliardi, L. Influence of First and Second Coordination Environment on Structural Fe(II) Sites in MIL-101 for C−H Bond Activation in Methane. *ACS Catal.* **2021**, *11* (2), 579−589.

(11) Barona, M.; Ahn, S.; Morris, W.; Hoover, W.; Notestein, J. M.; Farha, O. K.; Snurr, R. Q. Computational Predictions and Experimental Validation of Alkane Oxidative Dehydrogenation by Fe2M MOF Nodes. *ACS Catal.* **2020**, *10* (2), 1460−1469.

(12) Barona, M.; Snurr, R. Q. Exploring the Tunability of Trimetallic MOF Nodes for Partial Oxidation of Methane to Methanol. *ACS Appl. Mater. Interfaces* **2020**, *12* (25), 28217−28231.

(13) Hall, J. N.; Bollini, P. Low-Temperature, Ambient Pressure Oxidation of Methane to Methanol Over Every Tri-Iron Node in a Metal−Organic Framework Material. *Chem.—Eur. J.* **2020**, *26* (70), 16639−16643.

(14) Xiao, D. J.; Bloch, E. D.; Mason, J. A.; Queen, W. L.; Hudson, M. R.; Planas, N.; Borycz, J.; Dzubak, A. L.; Verma, P.; Lee, K.; et al. Oxidation of ethane to ethanol by N2O in a metal−organic framework with coordinatively unsaturated iron(II) sites. *Nat. Chem.* **2014**, *6* (7), 590−595.

(15) Dhakshinamoorthy, A.; Alvaro, M.; Horcajada, P.; Gibson, E.; Vishnuvarthan, M.; Vimont, A.; Grenèche, J. M.; Serre, C.; Daturi, M.; Garcia, H. Comparison of Porous Iron Trimesates Basolite F300 and MIL-100(Fe) As Heterogeneous Catalysts for Lewis Acid and Oxidation Reactions: Roles of Structural Defects and Stability. *ACS Catal.* **2012**, *2* (10), 2060−2065.

(16) Guesh, K.; Caiuby, C. A. D.; Mayoral, Á.; Díaz-García, M.; Díaz, I.; Sanchez-Sanchez, M. Sustainable Preparation of MIL-100(Fe) and Its Photocatalytic Behavior in the Degradation of Methyl Orange in Water. *Cryst. Growth Des.* **2017**, *17* (4), 1806−1813.

(17) Snyder, B. E. R.; Bols, M. L.; Schoonheydt, R. A.; Sels, B. F.; Solomon, E. I. Iron and Copper Active Sites in Zeolites and Their Correlation to Metalloenzymes. *Chem. Rev.* **2018**, *118* (5), 2718−2768.

(18) Fitzpatrick, P. F. Mechanism of aromatic amino acid hydroxylation. *Biochemistry* **2003**, *42* (48), 14083−14091.

(19) Neidig, M. L.; Decker, A.; Choroba, O. W.; Huang, F.; Kavana, M.; Moran, G. R.; Spencer, J. B.; Solomon, E. I. Spectroscopic and electronic structure studies of aromatic electrophilic attack and hydrogen-atom abstraction by non-heme iron enzymes. *Proc. Natl. Acad. Sci. U.S.A.* **2006**, *103* (35), 12966−12973.

(20) Tomaszewski, J. E.; Jerina, D. M.; Daly, J. W. Deuterium isotope effects during formation of phenols by hepatic monoxygenases. Evidence for an alternative to the arene oxide pathway. *Biochemistry* **1975**, *14* (9), 2024−2031.

(21) de Visser, S. P.; Shaik, S. A Proton-Shuttle Mechanism Mediated by the Porphyrin in Benzene Hydroxylation by Cytochrome P450 Enzymes. *J. Am. Chem. Soc.* **2003**, *125* (24), 7413−7424.

(22) Notté, P. P. The AlphOxTM process or the one-step hydroxylation of benzene into phenol by nitrous oxide. Understanding and tuning the ZSM-5 catalyst activities. *Top. Catal.* **2000**, *13* (4), 387−394.

(23) Bathelt, C. M.; Ridder, L.; Mulholland, A. J.; Harvey, J. N. Mechanism and structure−reactivity relationships for aromatic hydroxylation by cytochrome P450. *Org. Biomol. Chem.* **2004**, *2* (20), 2998−3005.

(24) Bathelt, C. M.; Ridder, L.; Mulholland, A. J.; Harvey, J. N. Aromatic Hydroxylation by Cytochrome P450: Model Calculations of Mechanism and Substituent Effects. *J. Am. Chem. Soc.* **2003**, *125* (49), 15004−15005.

(25) Jerina, D. M.; Daly, J. W. Arene Oxides: A New Aspect of Drug Metabolism. *Science* **1974**, *185* (4151), 573−582.

(26) Guroff, G.; Renson, J.; Udenfriend, S.; Daly, J. W.; Jerina, D. M.; Witkop, B. Hydroxylation-Induced Migration: The NIH Shift. *Science* **1967**, *157* (3796), 1524−1530.

(27) Snyder, B. E. R.; Bols, M. L.; Rhoda, H. M.; Vanelderen, P.; Böttger, L. H.; Braun, A.; Yan, J. J.; Hadt, R. G.; Babicz, J. T.; Hu, M. Y.; et al. Mechanism of selective benzene hydroxylation catalyzed by iron-containing zeolites. *Proc. Natl. Acad. Sci. U.S.A.* **2018**, *115* (48), 12124−12129.

(28) Gregg, S. J.; Sing, K. S. W. *Adsorption, Surface Area and Porosity*, 2nd ed.; Academic Press Inc.: London, 1982.

https://doi.org/10.1021/acs.jpcc.3c06423
J. Phys. Chem. C 2023, 127, 23246−23257

(29) Langmuir, I. The Adsorption of Gases on Plane Surfaces of Glass, Mica and Platinum. *J. Am. Chem. Soc.* **1918**, *40*, 1361−1403.
(30) Frisch, M. J.; Trucks, G. W.; Schlegel, H. B.; Scuseria, G. E.; Robb, M. A.; Cheeseman, J. R.; Scalmani, G.; Barone, V.; Petersson, G. A.; Nakatsuji, H.; et al. *Gaussian 16* Rev. B.01; Gaussian: Wallingford, CT, 2016.
(31) Zhao, Y.; Truhlar, D. G. The M06 suite of density functionals for main group thermochemistry, thermochemical kinetics, noncovalent interactions, excited states, and transition elements: two new functionals and systematic testing of four M06-class functionals and 12 other functionals. *Theor. Chem. Acc.* **2008**, *120* (1−3), 215−241.
(32) Weigend, F. Accurate Coulomb-fitting basis sets for H to Rn. *Phys. Chem. Chem. Phys.* **2006**, *8* (9), 1057−1065.
(33) Weigend, F.; Ahlrichs, R. Balanced basis sets of split valence, triple zeta valence and quadruple zeta valence quality for H to Rn: Design and assessment of accuracy. *Phys. Chem. Chem. Phys.* **2005**, *7* (18), 3297−3305.
(34) Verma, P.; Vogiatzis, K. D.; Planas, N.; Borycz, J.; Xiao, D. J.; Long, J. R.; Gagliardi, L.; Truhlar, D. G. Mechanism of Oxidation of Ethane to Ethanol at Iron(IV)−Oxo Sites in Magnesium-Diluted Fe2(dobdc). *J. Am. Chem. Soc.* **2015**, *137* (17), 5770−5781.
(35) Afeefy, H. Y.; Liebman, J. F.; Stein, S. E. Neutral Thermochemical Data. In *NIST Chemistry WebBook, NIST Standard Reference Database Number 69*, Mallard, P. J. L. a. W. G., Ed.; National Institute of Standards and Technology: Gaithersburg MD, 2023; p 20899.
(36) Snyder, B. E. R.; Böttger, L. H.; Bols, M. L.; Yan, J. J.; Rhoda, H. M.; Jacobs, A. B.; Hu, M. Y.; Zhao, J.; Alp, E. E.; Hedman, B.; et al. Structural characterization of a non-heme iron active site in zeolites that hydroxylates methane. *Proc. Natl. Acad. Sci. U.S.A.* **2018**, *115* (18), 4565−4570.
(37) Perdew, J. P.; Burke, K.; Ernzerhof, M. Generalized Gradient Approximation Made Simple. *Phys. Rev. Lett.* **1996**, *77* (18), 3865−3868.
(38) Kresse, G.; Furthmüller, J. Efficiency of ab-initio total energy calculations for metals and semiconductors using a plane-wave basis set. *Comput. Mater. Sci.* **1996**, *6* (1), 15−50.
(39) Grimme, S.; Antony, J.; Ehrlich, S.; Krieg, H. A consistent and accurate ab initio parametrization of density functional dispersion correction (DFT-D) for the 94 elements H-Pu. *J. Chem. Phys.* **2010**, *132* (15), 154104.
(40) Boys, S. F.; Bernardi, F. The calculation of small molecular interactions by the differences of separate total energies. Some procedures with reduced errors. *Mol. Phys.* **1970**, *19*, 553−566.
(41) De Moor, B. A.; Reyniers, M.-F.; Marin, G. B. Physisorption and chemisorption of alkanes and alkenes in H-FAU: a combined ab initio−statistical thermodynamics study. *Phys. Chem. Chem. Phys.* **2009**, *11* (16), 2939−2958.
(42) Grimme, S. Supramolecular Binding Thermodynamics by Dispersion-Corrected Density Functional Theory. *Chem.—Eur. J.* **2012**, *18* (32), 9955−9964.
(43) Ribeiro, R. F.; Marenich, A. V.; Cramer, C. J.; Truhlar, D. G. Use of Solution-Phase Vibrational Frequencies in Continuum Models for the Free Energy of Solvation. *J. Phys. Chem. B* **2011**, *115* (49), 14556−14562.
(44) Zhao, Y.; Truhlar, D. G. Computational characterization and modeling of buckyball tweezers: density functional study of concave−convex $\pi\cdots\pi$ interactions. *Phys. Chem. Chem. Phys.* **2008**, *10* (19), 2813−2818.
(45) John, M.; Alexopoulos, K.; Reyniers, M.-F.; Marin, G. B. Mechanistic insights into the formation of butene isomers from 1-butanol in H-ZSM-5: DFT based microkinetic modelling. *Catal. Sci. Technol.* **2017**, *7* (5), 1055−1072.
(46) Isley, W. 2023 https://github.com/william-isley-3rd/Comp-Chem-Toolwebs (accessed April 15, 2023).
(47) de Visser, S. P.; Oh, K.; Han, A.-R.; Nam, W. Combined Experimental and Theoretical Study on Aromatic Hydroxylation by Mononuclear Nonheme Iron(IV)−Oxo Complexes. *Inorg. Chem.* **2007**, *46* (11), 4632−4641.
(48) Kumar, D.; de Visser, S. P.; Sharma, P. K.; Cohen, S.; Shaik, S. Radical Clock Substrates, Their C−H Hydroxylation Mechanism by Cytochrome P450, and Other Reactivity Patterns: What Does Theory Reveal about the Clocks' Behavior? *J. Am. Chem. Soc.* **2004**, *126* (6), 1907−1920.
(49) de Visser, S. P. The axial ligand effect of oxo-iron porphyrin catalysts. How does chloride compare to thiolate? *J. Biol. Inorg. Chem.* **2006**, *11* (2), 168−178.
(50) Blanksby, S. J.; Ellison, G. B. Bond Dissociation Energies of Organic Molecules. *Acc. Chem. Res.* **2003**, *36* (4), 255−263.
(51) Horcajada, P.; Surble, S.; Serre, C.; Hong, D.-Y.; Seo, Y.-K.; Chang, J.-S.; Greneche, J.-M.; Margiolaki, I.; Ferey, G. Synthesis and catalytic properties of MIL-100(Fe), an iron(iii) carboxylate with large pores. *Chem. Commun.* **2007**, *27*, 2820−2822.
(52) Leclerc, H.; Vimont, A.; Lavalley, J.-C.; Daturi, M.; Wiersum, A. D.; Llwellyn, P. L.; Horcajada, P.; Ferey, G.; Serre, C. Infrared study of the influence of reducible iron(iii) metal sites on the adsorption of CO, CO2, propane, propene and propyne in the mesoporous metal-organic framework MIL-100. *Phys. Chem. Phys. Chem.* **2011**, *13* (24), 11748−11756.
(53) Yoon, J. W.; Seo, Y.-K.; Hwang, Y. K.; Chang, J.-S.; Leclerc, H.; Wuttke, S.; Bazin, P.; Vimont, A.; Daturi, M.; Bloch, E.; et al. Controlled Reducibility of a Metal−Organic Framework with Coordinatively Unsaturated Sites for Preferential Gas Sorption. *Angew. Chem., Int. Ed.* **2010**, *49* (34), 5949−5952.
(54) Wuttke, S.; Bazin, P.; Vimont, A.; Serre, C.; Seo, Y.-K.; Hwang, Y. K.; Chang, J.-S.; Férey, G.; Daturi, M. Discovering the Active Sites for C3 Separation in MIL-100(Fe) by Using Operando IR Spectroscopy. *Chem.—Eur. J.* **2012**, *18* (38), 11959−11967.
(55) Vitillo, J. G.; Gagliardi, L. Thermal Treatment Effect on CO and NO Adsorption on Fe(II) and Fe(III) Species in Fe(3)O-Based MIL-Type Metal-Organic Frameworks: A Density Functional Theory Study. *Inorg. Chem.* **2021**, *60* (16), 11813−11824.
(56) Meng, L.; Zhu, X.; Hensen, E. J. M. Stable Fe/ZSM-5 Nanosheet Zeolite Catalysts for the Oxidation of Benzene to Phenol. *ACS Catal.* **2017**, *7* (4), 2709−2719.
(57) Li, G.; Pidko, E. A.; van Santen, R. A.; Feng, Z.; Li, C.; Hensen, E. J. M. Stability and reactivity of active sites for direct benzene oxidation to phenol in Fe/ZSM-5: A comprehensive periodic DFT study. *J. Catal.* **2011**, *284* (2), 194−206.
(58) Eubank, J. F.; Wheatley, P. S.; Lebars, G.; McKinlay, A. C.; Leclerc, H.; Horcajada, P.; Daturi, M.; Vimont, A.; Morris, R. E.; Serre, C. Porous, rigid metal(III)-carboxylate metal-organic frameworks for the delivery of nitric oxide. *APL Mater.* **2014**, *2* (12), 124112.
(59) Korzekwa, K. R.; Swinney, D. C.; Trager, W. F. Isotopically labeled chlorobenzenes as probes for the mechanism of cytochrome P-450 catalyzed aromatic hydroxylation. *Biochemistry* **1989**, *28* (23), 9019−9027.
(60) Kaizer, J.; Klinker, E. J.; Oh, N. Y.; Rohde, J.-U.; Song, W. J.; Stubna, A.; Kim, J.; Münck, E.; Nam, W.; Que, L. Nonheme $Fe^{IV}O$ Complexes That Can Oxidize the C−H Bonds of Cyclohexane at Room Temperature. *J. Am. Chem. Soc.* **2004**, *126* (2), 472−473.
(61) Oh, N. Y.; Suh, Y.; Park, M. J.; Seo, M. S.; Kim, J.; Nam, W. Mechanistic Insight into Alcohol Oxidation by High-Valent Iron−Oxo Complexes of Heme and Nonheme Ligands. *Angew. Chem., Int. Ed.* **2005**, *44* (27), 4235−4239.
(62) Dubkov, K. A.; Sobolev, V. I.; Talsi, E. P.; Rodkin, M. A.; Watkins, N. H.; Shteinman, A. A.; Panov, G. I. Kinetic isotope effects and mechanism of biomimetic oxidation of methane and benzene on FeZSM-5 zeolite. *J. Mol. Catal. Chem.* **1997**, *123* (2−3), 155−161.
(63) Korzekwa, K.; Trager, W.; Gouterman, M.; Spangler, D.; Loew, G. Cytochrome P450 mediated aromatic oxidation: a theoretical study. *J. Am. Chem. Soc.* **1985**, *107* (14), 4273−4279.
(64) Jerina, D. M.; Daly, J. W.; Witkop, B.; Zaltzman-Nirenberg, P.; Udenfriend, S. The role of arene oxide-oxepin systems in the metabolism of aromatic substrates. III. Formation of 1,2-naphthalene oxide from naphthalene by liver microsomes. *J. Am. Chem. Soc.* **1968**, *90* (23), 6525−6527.

https://doi.org/10.1021/acs.jpcc.3c06423
J. Phys. Chem. C 2023, 127, 23246−23257

(65) Curet-Arana, M. C.; Snurr, R. Q.; Broadbelt, L. J. Quantum Chemical Analysis of the Reaction Pathway for Styrene Epoxidation Catalyzed by Mn-Porphyrins. In *Mechanisms in Homogeneous and Heterogeneous Epoxidation Catalysis*, Oyama, S. T., Ed.; Elsevier: Amsterdam, 2008; Chapter 19, pp 471−486.
(66) Nam, W. High-Valent Iron(IV)−Oxo Complexes of Heme and Non-Heme Ligands in Oxygenation Reactions. *Acc. Chem. Res.* **2007**, *40* (7), 522−531.
(67) Kachurovskaya, N. A.; Zhidomirov, G. M.; Hensen, E. J. M.; van Santen, R. A. Cluster Model DFT Study of the Intermediates of Benzene to Phenol Oxidation by N2O on FeZSM-5 Zeolites. *Catal. Lett.* **2003**, *86* (1/3), 25−31.
(68) Periana, R. A.; Taube, D. J.; Evitt, E. R.; Löffler, D. G.; Wentrcek, P. R.; Voss, G.; Masuda, T. A Mercury-Catalyzed, High-Yield System for the Oxidation of Methane to Methanol. *Science* **1993**, *259* (5093), 340−343.
(69) Latimer, A. A.; Kakekhani, A.; Kulkarni, A. R.; Nørskov, J. K. Direct Methane to Methanol: The Selectivity−Conversion Limit and Design Strategies. *ACS Catal.* **2018**, *8*, 6894−6907.
(70) Ravi, M.; Ranocchiari, M.; van Bokhoven, J. A. The Direct Catalytic Oxidation of Methane to Methanol—A Critical Assessment. *Angew. Chem., Int. Ed.* **2017**, *56* (52), 16464−16483.

https://doi.org/10.1021/acs.jpcc.3c06423
J. Phys. Chem. C 2023, 127, 23246−23257